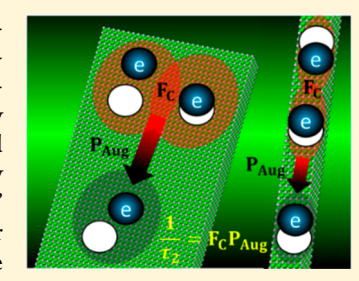
Size- and Morphology-Dependent Auger Recombination in CsPbBr₃ Perovskite Two-Dimensional Nanoplatelets and One-Dimensional **Nanorods**

Qiuyang Li,^{†,§®} Yawei Yang,^{†,‡,§} Wenxiu Que,^{‡®} and Tianquan Lian*,^{†®}

Supporting Information

Downloaded via EMORY UNIV on October 3, 2019 at 17:38:06 (UTC). See https://pubs.acs.org/sharingguidelines for options on how to legitimately share published articles.

ABSTRACT: CsPbX₃ (X = Cl, Br, I) perovskite nanocrystals (NCs), including zerodimensional (0D) quantum dots (QDs), one-dimensional (1D) nanorods (NRs), and twodimensional (2D) nanoplatelets (NPLs), have shown promising performances in lightemitting diode (LED) and lasing applications. However, Auger recombination, one of the key processes that limit their performance, remains poorly understood in CsPbX₃ 2D NPLs and 1D NRs. We show that the biexciton Auger lifetimes of CsPbBr₃ NPLs (NRs) scale linearly with the NPL lateral area (NR length) and deviates from the "universal volume scale law" that has been observed for QDs. These results are consistent with a model in which the Auger recombination rate for 1D NRs and 2D NPLs is a product of binary collision frequency in the nonquantum confined dimension and Auger probability per collision. Comparisons of Auger



recombination in CsPbBr₃ NCs of different dimensionalities and similar band gaps suggest that Auger probability increases in NCs with a higher number of confined dimensions. Compared to CdSe and PbSe NCs with the same dimensionalities and similar sizes, Auger recombination rates in 0D-2D CsPbBr₃ NCs are over 10-fold faster. Fast Auger recombination in CsPbBr₃ NCs shows their potentials for Auger-assisted up-conversion and single photon source, while suppressing Auger recombination may further enhance their performances in LED and lasing applications.

KEYWORDS: Perovskite, nanoplatelets, nanorods, multiple excitons, Auger recombination, biexciton lifetime

Metal-halide perovskite materials (APb X_3 , where A = methylammonium or Cs and X = Cl, Br, I) have shown great potentials for optoelectrical applications, 1-3 because they possess a high luminescent quantum yield, long charge carrier lifetime, and long carrier diffusion length.⁴ For example, the solar-to-electricity conversion efficiency of the best-reported perovskite solar cells exceeds 20%. $^{5-14}$ Recently, CsPbX₃ (X = Cl, Br, I) nanocrystals (NCs), including zero-dimensional (0D) quantum dots (QDs), 15-19 one-dimensional (1D) nanorods (NRs),^{20,21} and two-dimensional (2D) nanoplatelets (NPLs)²²⁻³⁰ have been reported. Compared to their bulk counterparts, CsPbX₃ QDs have both size- and anion-tunable emission that covers the whole visible region (400-700 nm) with a luminescent quantum yield as high as ~90% and can be synthesized facilely via solution methods. 16 In addition, CsPbX₃ NRs and NPLs have strongly bound excitons (>100 meV binding energy) with a larger transition oscillator strength and sharp emission peaks. 20,30,31 These properties make CsPbX₃ $\stackrel{\frown}{N}$ Cs even more promising materials for light-emitting diodes (LEDs)^{32–39} and lasing,^{40–44} than their bulk counterparts.

Optoelectrical applications in LEDs and lasing require multicarrier or exciton radiative recombination, while photovoltaics require multicharge separation. These processes compete with the deactivation of multiple exciton states by Auger recombination, in which one electron-hole pair recombines nonradiatively by exciting another carrier into a higher energy level. The rate of this process is enhanced in quantum-confined NCs due to the relaxation of momentum conservation requirement. 45,46 Thus, understanding and controlling Auger recombination in NCs are essential for the rational design and improvements of their optoelectrical performances. For example, direct-current electrical pumped optical gain has been achieved using engineered cadmium chalcogenide QD film with suppressed Auger recombination. 47 A reported amplified spontaneous emission threshold (\sim 6 μ J/ cm²) of 2D CdSe NPLs^{48,49} is an order of magnitude lower than that in similar QDs $(\sim 6 \text{ mJ/cm}^2)^{50}$ due partially to the longer Auger recombination lifetime in 2D NPLs. Despite its importance, how the Auger recombination times in CsPbX₃ 2D NPLs and 1D NRs depend on size and morphology has yet to be reported.

Herein, we report a study of the Auger recombination lifetime of colloidal CsPbBr3 NPLs and NRs with different

Received: May 26, 2019 Revised: June 23, 2019 Published: June 27, 2019

Department of Chemistry, Emory University, 1515 Dickey Drive, NE, Atlanta, Georgia 30322, United States

[‡]Electronic Materials Research Laboratory, Key Laboratory of the Ministry of Education, International Center for Dielectric Research, and Shaanxi Engineering Research Center of Advanced Energy Materials and Devices, School of Electronic and Information Engineering, Xi'an Jiaotong University, Xi'an 710049, Shaanxi People's Republic of China

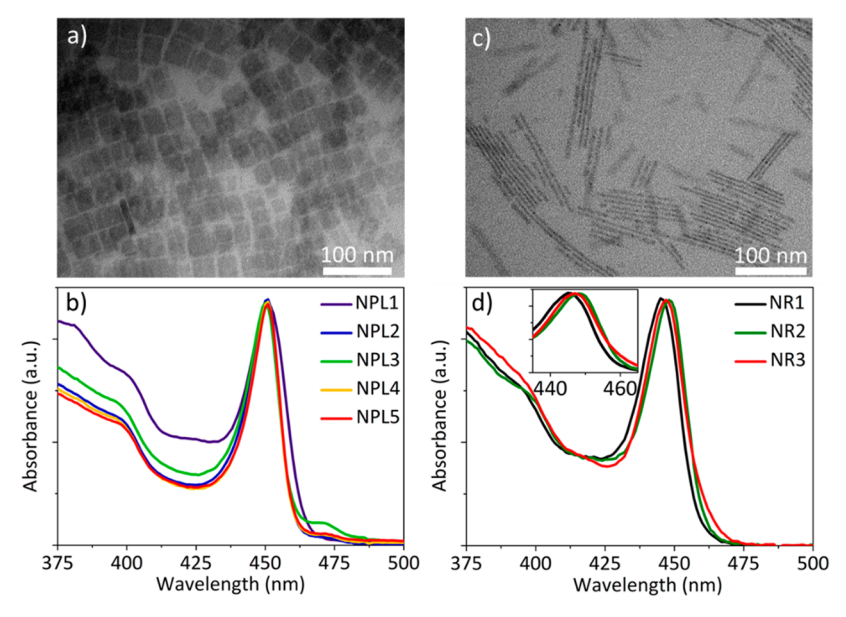


Figure 1. CsPbBr₃ NPLs and NRs. (a) TEM image of NPL3. (b) Normalized absorption spectra of NPL1-5. (c) TEM image of NR3. (d) Normalized absorption spectra of NR1-3. Inset: Expanded view of the absorption spectra at the exciton peak region (435-465 nm).

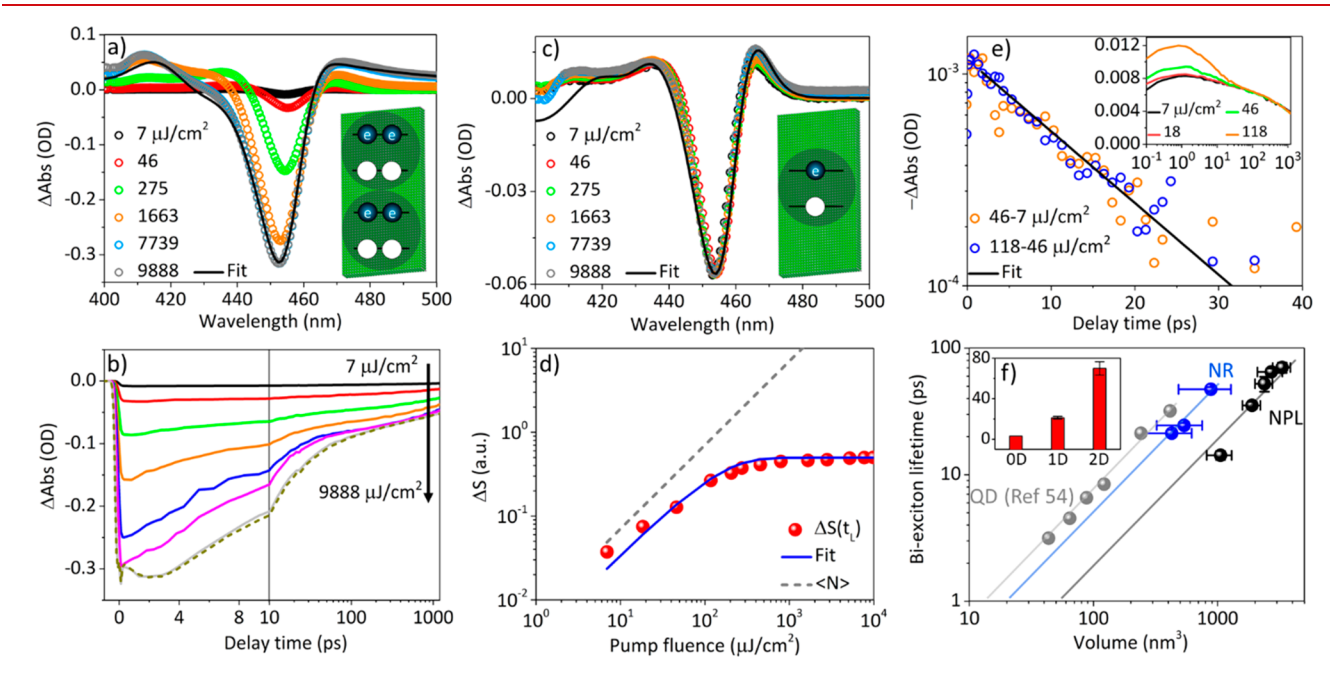


Figure 2. Auger recombination in CsPbBr₃ NPLs and NRs. (a) TA spectra of NPL1 at early delay time $(t_E, 1-2 \text{ ps})$ at indicated pump fluences (circles). The black solid line is the fit of the TA spectra at 9888 μ J/cm². Inset: Schematics of the multiexciton state with a saturated number of band-edge excitons. (b) XB kinetics of NPL1 at different pump fluences. (c) Normalized TA spectra of NPL1 at long delay time $(t_L, 800-1000 \text{ ps})$ at indicated pump fluences (circles). Black solid line is the fit of the TA spectra at 9888 μ J/cm². Inset: Schematics of a single exciton state. (d) Normalized XB amplitude at t_L as a function of pump fluence (red spheres), its fit according to a Poisson distribution model described in SI section S3 (blue solid line), and the average total exciton number per NPL $(\langle N \rangle)$ as a function of pump fluence (gray dashed line). (e) Extracted biexciton decay kinetics (circles) and their single-exponential fit (black solid line). Inset: Normalized XB kinetics at low pump fluences (<118 μ J/cm²). (f) Biexciton lifetime of CsPbBr₃ NPLs (black spheres), NRs (blue spheres), and QDs (gray spheres) as a function of their volume (V). The biexciton lifetimes of CsPbBr₃ QDs with different volumes are adapted from ref 54. The solid lines are the linear fits to the volume-dependent biexciton lifetime of QDs, NRs, and NPLs, respectively. Inset: Comparison of biexciton lifetime of OD, 1D, and 2D NCs with similar band gap, diameter (or thickness of NPLs), and length (of NRs and NPLs).

lateral areas and rod lengths, respectively, via transient absorption (TA) spectroscopy. The biexciton Auger lifetime of CsPbBr₃ NPLs and NRs scales linearly with the NPL lateral area and the NR length, respectively, consistent with an Auger recombination model reported previously. This model is used to analyze how the Auger recombination rate depends on

the morphology of CsPbBr₃ NCs. Furthermore, this model enables a comparison of Auger recombination times with CdSe and PbSe NCs of the same morphology and similar sizes, revealing the dependence of Auger recombination probabilities on material compositions.

Sample Characterization. CsPbBr₃ NPLs with 5 monolayers (ML) of unit cells and varying lateral areas were synthesized following reported procedures with slight modifications. 24,28,29 Synthesis details are provided in Supporting Information (SI) section S1. These NPL samples are dispersed in hexane and labeled as NPL1-5 with increasing lateral areas, which were determined from their transmission electron microscopy (TEM) images (Figure 1a for NPL3 and Figure S1a-d for the remaining NPL samples). These CsPbBr₃ NPLs show a rectangular shape and an average lateral area (S_{NPL}) from 352.0 ± 80.0 to 1104.3 ± 180.0 nm² (Table S1). The NPL thickness can be well characterized by the exciton peak position (~450 nm) in the absorption spectra (Figure 1b) and is estimated to be ~3 nm based on the characterization reported in literature.²⁴ Note that the TEM images of some NPL samples show the presence of small particles and voids (Figure S1b-d), which can be attributed to the reduction of Pb²⁺ to Pb nanoparticles from NCs under the electron beam of TEM characterization, ⁵² and has also been observed previously in CsPbBr₃ QDs, ⁵² NRs, ⁵² and NPLs. ^{24,53} The normalized absorption spectra of NPL1-5 (Figure 1b) show an pronounced band-edge exciton peak at ~450 nm.²⁴ Both exciton absorption and photoluminescence (PL, Figure S4) peaks show negligible shifts among different NPL samples, confirming that their thicknesses are the same. Some NPL samples also show a small absorption and emission peak (Figure S4) below the main exciton peak, which is attributed to the presence of a small amount of thicker NPLs with a smaller band gap. ^{24,28,29} CsPbBr₃ NRs with similar diameters and different rod lengths were synthesized following reported procedures with slight modifications (see SI section S1 for details).20 These NR samples are dispersed in hexane and labeled as NR1-3 with increasing rod lengths. Figure 1c and Figure S1e,f show the TEM images of NR3 and NR1-2, respectively, from which the rod diameters and length (in parentheses) for NR samples are determined to be 3.1 ± 0.6 (42.7 ± 9.0) , 3.4 ± 0.7 (46.7 ± 9.4) , and 3.2 ± 0.5 (83.7 ± 9.4) 25.0) nm for NR1-3, respectively (Table S2). Figure 1d shows the normalized absorption spectra of NR1-3, where their exciton peaks center at ~445, ~448, and ~447 nm, respectively (inset of Figure 1d).

Size-Dependent Auger Recombination Lifetime. We carried out pump fluence-dependent TA spectroscopy on CsPbBr₃ NPL and NR solution samples (in a cuvette with 1 mm light path) to quantify their Auger recombination lifetimes. All samples were excited at 400 nm in this work. Figure 2a shows the TA spectra of NPL1 (circles) at early delay time $(t_E, 1-2 \text{ ps})$ with different pump fluences. According to our previous study on CsPbBr3 NPLs, the exciton bleach (XB), the negative peak centered at ~450 nm, is induced by the band-edge exciton state-filling with an electron at the conduction band (CB) edge and a hole at the valence band (VB) edge, directly probing the population of band-edge excitons.³⁰ Figure 2b shows the XB kinetics at different pump fluences. The XB amplitude reaches the maximum at $t_{\rm E}$ (1–2 ps) when the band-edge exciton formation is completed and multiexciton annihilation is negligible. With increasing pump fluence, more NPLs in solution are excited, and more bandedge excitons are generated per NPL so that XB amplitude (at $t_{\rm E}$) grows with pump fluence until the band-edge exciton states in NPLs are fully occupied at 7739 μ J/cm² or higher (inset of Figure 2a). The TA spectra at t_E show different spectral features (Figure 2a), reflecting the presence of different

multiple exciton states, and the amplitudes of faster decay component in the XB kinetics (Figure 2b) also increases, indicating a larger contribution of shorter lived multiexciton states. Figure 2c shows the comparison of TA spectra at long delay time ($t_{\rm L}$, 800–1000 ps) measured with different pump fluences. These normalized TA spectra at t_L show identical spectral shape, indicating that multiexciton annihilation is completed at t_1 and only single exciton states remain in excited NPLs (inset of Figure 2c). Therefore, XB amplitude at the $t_{\rm L}$ probes the population of excited NPLs and can be directly related to the probability of finding excited NPLs ($\Delta S(t_L)$) by a scaling factor α . As shown in Figure 2d, $\Delta S(t_L)$ of NPL1 as a function of pump fluence can be fitted to a Poisson distribution model.⁵¹ This fit also reveals the average number of absorbed photons per NPL, $\langle N \rangle$, which increases with the pump fluence (gray dashed line in Figure 2d), confirming the presence of multiple exciton states at high pump fluence. The details of the model and fitting procedure can be found in the SI section S3.

A comparison of XB kinetics measured at low fluences and normalized at t_L (inset of Figure 2e) shows that at low pump fluence ($<18 \mu J/cm^2$), the normalized XB kinetics are independent on the pump fluence, indicating that these signals are dominated by single-exciton kinetics. At higher pump fluence (>46 μ J/cm²), the kinetics show an additional faster decay component that can be attributed to biexciton decay. At 46 $\mu J/cm^2$, the estimated $\langle N \rangle$ is ~0.32, and according to Poisson distribution, the percentage of NPLs with single-, bi-, and higher-exciton (>2) states among all excited NPLs are ~84.8%, ~13.6%, and ~1.6%, respectively, indicating singleand biexciton decay dominates the XB kinetics. Thus, biexciton decay kinetics (orange circles in Figure 2e) can be extracted by subtracting the normalized single-exciton kinetics at $7 \mu \text{J/cm}^2$ from the normalized total kinetics at 46 μ J/cm². Subtraction of normalized XB kinetics at 118 μ J/cm² by that at 46 μ J/cm² also gives the same decay kinetics (blue circles in Figure 2e), confirming that the additional fast decay component is dominated by biexciton decay at these low fluences (<118 μ J/cm²). This kinetics subtraction method has been used to extract biexciton lifetimes of other 0D-2D NCs, 17,47,51,54,55 and the details of this method are described in SI section S4. Biexciton decay kinetics of NPL1 can be well fit by a singleexponential decay (solid line in Figure 2e) with a time constant (τ_2) of 14.2 \pm 1.2 ps. It is important to note the solution samples were vigorously stirred during the TA measurements to avoid photocharging effect, which can produce trions and other species. 17,56-58 Biexciton decay contains biexciton radiative decay and nonradiative Auger recombination. The biexciton radiative decay time is estimated to be half of the single-exciton radiative decay time $(\tau_{X,r})$ because biexcitons have two radiative decay channels.⁵⁹ XB kinetics at $7 \mu \text{J/cm}^2$ contains both radiative and nonradiative single-exciton decay processes, thus, the half-life of XB kinetics at 7 μ J/cm² ($\tau_{\rm X}$ ~ 1000 ps) provides the lower limit of the single-exciton radiative decay half-life: $\tau_{\rm X} < \tau_{\rm X,r}$. Since the half-life of biexciton decay $(9.84 \pm 0.50 \text{ ps})$ is much shorter than $\tau_x/2$ $(\langle \tau_{x_x}/2 \rangle)$, nonradiative Auger recombination dominates the biexciton decay in NPL1, and τ_2 can be taken as the biexciton Auger recombination lifetime.

Using the same method, we extracted the biexciton Auger lifetime of all NPL and NR samples, which are plotted as a function of NC volume (V) in Figure 2f. The relevant TA spectra and kinetics of all NR and other NPL samples are shown in SI sections S3 and S4 (Figure S5–S8). The volume

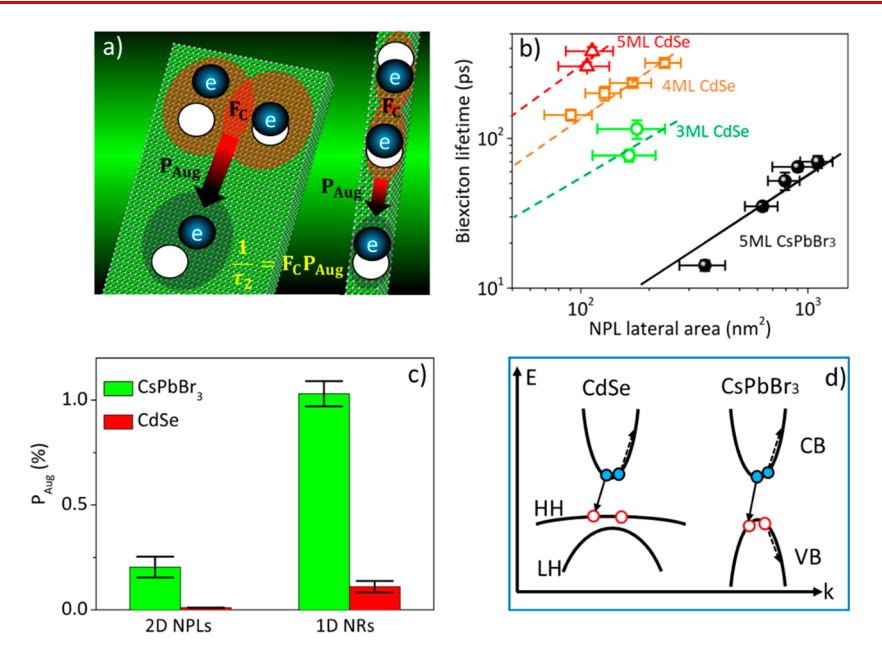


Figure 3. Comparison of Auger recombination in CdSe and CsPbBr₃ NPLs. (a) Scheme of Auger recombination model in CsPbBr₃ NPLs (left) and NRs (right). F_C is the binary exciton collision frequency, and P_{Aug} is the Auger probability per collision. (b) Biexciton lifetime of 5 ML CsPbBr₃ NPLs and CdSe NPLs with different thicknesses as a function of NPL lateral area. The biexciton lifetimes of CdSe NPLs are adapted from ref 51. The solid and dashed lines are the linear fits. (c) Morphology- and material-dependent Auger probability per collision (P_{Aug}). (d) Scheme of the band structures of CdSe and CsPbBr₃ NPLs. HH and LH represent heavy hole and light hole bands in CdSe NPLs, respectively.

of NRs is calculated by assuming a cuboid morphology with a square cross-section and a long rod length due to the cubic perovskite structure. 20,52 The biexciton lifetimes of CsPbBr₃ QDs (gray spheres, from ref 54) are also compared in Figure 2f, which scales linearly with their volume (gray dashed line). It should be noted that it has been reported that the biexciton lifetime of a set of larger CsPbBr3 QDs scales sublinearly to their volume $(V^{0.5})$, 17 and the different volume dependence has been attributed to a much weaker confinement in these larger QDs.⁵⁴ The results in Figure 2f suggest that the biexciton lifetimes of 0D QDs, 1D NRs, and 2D NPLs do not show a linear dependence on their volumes with the same slope, indicating that they do not obey a "universal volume scaling law" that has been reported for 0D QDs. 60-63 Thus, different models should be considered when comparing biexciton Auger lifetimes of NCs of different dimensionalities.

Morphology-Dependent Auger Recombination in CsPbBr₃ NCs. Extensive studies in 0D QDs have shown that the biexciton Auger rate $(1/\tau_2)$ follows the "universal volume scaling law":

$$\left(\frac{1}{\tau_2}\right)_{0D} = V_{QD} A_{Aug} \tag{1}$$

where $V_{\rm QD}$ is the QD volume and $A_{\rm Aug}$ is the biexciton Auger recombination rate per unit volume. According to our previous study, the biexciton Auger lifetime shows a dramatically different dependence on the sizes of the quantum-confined and the nonquantum-confined dimensions in CdSe NPLs, and volume is not a useful indicator (see SI section S5 for details). Exciton motion along the nonquantum-confined dimensions is diffusive, and the collision frequency of two excitons ($F_{\rm C}$) depends inversely with the areas of NPLs ($S_{\rm NPL}$). Auger recombination probability per collision ($P_{\rm Aug}$) depends strongly on the size of the quantum-confined dimension. The biexciton Auger recombination rate ($1/\tau_2$) is then the

product of collision frequency and Auger probability (Figure 3a), as shown in eq 2. A similar model can be extended to derive an expression of biexciton Auger lifetime of 1D NRs (with rod length of $L_{\rm NR}$), shown in eq 3:

$$\left(\frac{1}{\tau_2}\right)_{\rm 2D} = F_{\rm C} P_{\rm Aug} = \left(4\sqrt{\frac{S_{\rm X}}{\pi}} \frac{\overline{\nu}}{S_{\rm NPL}}\right) P_{\rm Aug} \tag{2}$$

$$\left(\frac{1}{\tau_2}\right)_{1D} = F_C P_{\text{Aug}} = \left(\frac{\overline{\nu}}{L_{\text{NR}}}\right) P_{\text{Aug}}$$
(3)

In eqs 2 and 3, $S_{\rm X}$ is the exciton center-of-mass (COM) coherent spatial area, and $\overline{\nu}$ is the average exciton diffusion velocity (see SI section S5 for Auger recombination model details).

Because these NPLs (NRs) have the same thicknesses (similar diameters), the results shown in Figure 2f suggest that biexciton lifetimes of NPLs (NRs) scale linearly with NPL lateral area (NR length), consistent with eqs 2 and 3. 51,65 As shown in the inset of Figure 2f, with a similar diameter (~3 nm) and band gap (~450 nm), the biexciton lifetime of NR1 (21.3 \pm 1.3 ps) is ~7-fold longer than that in QDs (~3.14 ps), 54 but is over 3-fold shorter than that of NPL5 (70.0 \pm 6.6 ps) with a similar length (42.7 \pm 9.0 nm for NR1 and 36.9 \pm 3.7 nm for NPL5). These results support a morphology-dependent Auger recombination.

To identify the origin of the morphological dependence of the Auger recombination rate in CsPbBr₃ 2D NPLs and 1D NRs, we estimate the exciton collision frequency (F_C) and extract the Auger probability (P_{Aug}) of 2D NPLs and 1D NRs using eqs 2 and 3, respectively. F_C is determined by the exciton COM coherent area (S_X) of CsPbBr₃ NPLs and the average exciton collision velocity ($\overline{\nu}$). Assuming 2D NPLs have a homogeneous quantum confinement along the thickness direction, S_X is determined by exciton—phonon scattering

and can be estimated as $S_X = 4\hbar^2/\Delta(T)M$, where \hbar is the Planck's constant, $\Delta(T)$ is the transition line width at temperature T, and M is the sum of the effective masses of the CB edge electron and VB edge hole.66-68 At room temperature, $\Delta(298 \text{ K})$ is considered as the emission line width of CsPbBr₃ NPLs (~70 meV as shown in Figure S4). With M of 5 ML CsPbBr₃ NPL reported as $\sim 0.4 m_0^{24}$ the estimated S_X for CsPbBr₃ NPLs is ~430 nm². The average exciton collision velocity $(\overline{\nu})$ in NCs are limited by the scattering with thermal phonons: $M\overline{v}^2/2=3k_BT/2$, where k_B is the Boltzmann constant and T is temperature (298 K).⁶⁹ Assuming the same $M (0.4 m_0)^{24}$ for both CsPbBr₃ NPLs and NRs, $\overline{\nu}$ can be estimated to be ~184 nm/ps for both NCs. 2D biexciton collision frequency is a factor of $2d/\sqrt{S_{\rm NPL}}$ larger than 1D collision frequency if $S_{\rm NPL} = L_{\rm NR}^{-2}$, where $d = 2\sqrt{S_{\rm X}/\pi}$ is the diameter of the exciton COM coherent area (see Figure S9). The value of $2d/\sqrt{S_{\rm NPL}}$ varies from ~1.2 to ~0.7 from NPL1-5, indicating the exciton collision frequency ratio between 2D and 1D is close to 1 and is not the dominant factor that determines morphology-dependent Auger recombination between 2D and 1D.

With the estimated F_C and the measured biexciton lifetimes, the value of $P_{\rm Aug}$ can be determined to be 0.204 \pm 0.050% and $1.03 \pm 0.06\%$ for CsPbBr₃ NPLs and NRs using eqs 2 and 3, respectively, as shown in Figure 3c. This \sim 5-fold larger P_{Aug} of CsPbBr₃ 1D NRs than that of 2D NPLs indicates that the morphology-dependent P_{Aug} is the key to different Auger recombination rates in 2D and 1D NCs. Although the reason for this morphology-dependent P_{Aug} remains unclear, P_{Aug} is determined by the wave function overlap among the four involved carriers: the recombined electron-hole pair, the additional carrier before Auger excitation, and the carrier on the higher energy level after Auger excitation.^{64,70} It has also been reported previously that the Auger recombination rates of CdSe NPLs and NRs scale with $(\sim z^{-7})^{51,64}$ and $(\sim d^{-3})^{70}$ respectively, where z is the thickness for NPLs and d is the diameter for NRs. The morphology-dependent Auger lifetimes in both CdSe and CsPbBr₃ NCs suggest that Auger probability increases with more degrees of quantum confinement in NCs of the same composition.

Enhanced Auger Probability in CsPbBr₃ NCs. It is interesting to compare the Auger recombination of CsPbBr₃ NCs to NCs with different chemical compositions and the same morphology. Figure 3b shows the comparison of the lateral area-dependent biexciton lifetimes of CsPbBr3 and CdSe NPLs of different thicknesses. The biexciton lifetime of CsPbBr₃ NPLs ranges from 14.2 ± 1.2 to 70.0 ± 6.6 ps, which is shorter than the reported value (100s of ps)⁵¹ of CdSe NPLs of smaller lateral areas. For example, for 5 ML CdSe NPLs with a thickness of ~1.7 nm⁷¹ and a lateral area of ~110 nm², the reported biexciton lifetime is ~300 ps,⁵¹ over 20-fold longer than that in 5 ML CsPbBr₃ NPLs (~14 ps) with a thickness of \sim 3 nm, ²⁴ and a 3-fold larger lateral area (\sim 352 nm²). Similarly, the biexciton lifetime of CsPbBr₃ NRs (ranges from 21.3 ± 1.3 to 47.3 ± 1.9 ps) is much shorter than that reported in CdSe^{72,73} and PbSe NRs⁵⁵ (100s of ps) of shorter rod lengths, and CsPbBr₃ QDs are also reported to have a 10-fold shorter biexciton lifetime compared to CdSe and PbSe QDs with similar volumes. 17,54

The Auger recombination lifetime in CsPbBr₃ QDs is 10 times faster than CdSe and PbSe QDs of similar volumes, ^{17,54} which according to eq 1 suggests that the Auger probability

 $(A_{\rm Aug})$ is 10 times larger in CsPbBr₃QDs. For 1D NRs and 2D NPLs, according to eqs 2 and 3, both $F_{\rm C}$ and $P_{\rm Aug}$ affect the Auger recombination rate. The estimated S_X of 5 ML CdSe NPLs is ~156 nm², ⁶⁸ and the estimated $\overline{\nu}$ of CdSe NPLs and NRs is ~ 115 nm/ps. Thus, assuming the same NC dimensions $(S_{\text{NPL}} \text{ and } L_{\text{NR}})$, the estimated F_{C} for CsPbBr₃ 2D NPLs and 1D NRs is ~2.7- and ~1.6- fold larger than those of CdSe NPLs and NRs according to eqs 2 and 3, respectively. P_{Aug} for CdSe 2D NPLs and 1D NRs is then estimated to be 0.010 \pm 0.001% and 0.111 \pm 0.027%, respectively, using the parameters $(S_{\rm NPL}, L_{\rm NR}, \text{ and } \tau_2)$ reported in NPL⁵¹ and NR literature,⁷³ which is ~20- and ~9.3-fold smaller than that of CsPbBr₃ 2D NPLs and 1D NRs, respectively, as shown in Figure 3c. These values suggest that larger Auger probability (P_{Aug} and A_{Aug}) is the key factor for faster Auger recombination rates in CsPbBr₃ 2D, 1D, and 0D NCs compared to CdSe NCs of the same dimensionalities and sizes. One possible explanation is the smaller effective mass of the VB hole in CsPbBr₃ compared to CdSe. As shown in Figure 3d, in biexciton Auger recombination, the annihilation of an exciton requires the excitation of a CB electron or VB hole to conserve both energy and momentum. Because of the small momentum of excitons, the momentum conservation requirement can be more easily satisfied by exciting carriers with a small effective mass. In CdSe NPLs, biexciton Auger recombination is dominated by the excitation of CB electron (with effective mass of $0.13m_0$), while the pathway involving excitation of a heavy hole (with effective mass of $0.9m_0$)⁷⁴ into a higher energy level in heavy hole band is less favorable. Moreover, the Auger recombination pathway involving the excitation of a heavy hole into the light hole band is also negiligble in CdSe NPLs because P_{Aug} for this process depends on the amplitude of heavy hole wave function at the NPL boundary, which is calculated to be small in 2D quantum wells with similar electronic structures.⁶⁴ However, in CsPbBr₃ NPLs, the effective mass for band-edge electrons and holes is similar and small (~0.2m₀),²⁴ leading to an additional Auger recombination pathway involving hole excitations (Figure 3d) compared with CdSe and an increased P_{Aug} . A more indepth understanding of the enhanced P_{Aug} (and A_{Aug}) in CsPbBr₃ NCs compared with conventional II-VI semiconductor NCs remains unclear and requires detailed theoretical studies. We hope that our results can stimulate more comprehensive theoretical studies that can quantitatively explain the enhanced Auger probability in perovskite NCs.

Despite fast Auger recombination in CsPbBr₃ NCs, promising performances in optoelectrical applications, such as LED^{32-39} and lasing, 40-44 have been reported for these materials. For NPL-based LEDs,⁷⁶ the reported maximum external quantum efficiency (EQE_{max} $\sim 0.1-1.1\%$) and onset voltage ($V_{\rm on}$, $\sim 3.8-4.0$ V) of CsPbBr₃^{32,77} are comparable to the reported values (~0.6-3.6% and ~1.9-5.5 V) of CdSe NPL-LED. 78-81 This indicates that other properties of CsPbBr₃ NCs may have compensated for the loss caused by fast Auger recombination in those optoelectrical applications. Possible factors may include the high PL quantum yield of CsPbBr₃ NCs, which can reach ~90% without passivation by an inorganic shell. 16 Our finding also suggests that suppressing Auger recombination in CsPbBr₃ NCs can be a potential way to further enhance their light emitting and lasing performances. In addition to size tuning (as shown in Figure 3b), another possible approach for extending Auger lifetime is to use organic cations in perovskite NCs. Ginger and co-workers have

reported that biexciton Auger recombination in CsPbBr₃ QDs is faster than that in hybrid perovskite QDs such as $CH_2(NH_2)_2PbBr_3$ and $CH_3NH_3PbI_3$ QDs with a similar size. This cation exchange method may also apply to 1D and 2D perovskite NCs. Moreover, the fast Auger recombination rate of CsPbBr₃ NCs may make them promising materials for Auger-assisted up-conversion 83,84 and a single photon emission source. $^{85-87}$

In summary, we have studied how biexciton Auger recombination lifetimes depend on size, morphology, and material composition in 0D, 1D, and 2D NCs. The biexciton Auger recombination lifetimes of CsPbBr3 NPLs and NRs increase linearly with NPL lateral areas and NR lengths, respectively. Comparison of the biexciton lifetimes of NRs and NPLs with the reported values of QDs shows that the "universal volume scaling law" does not apply to NCs of different dimensionalities. The failure of this simple scaling rule, which has been demonstrated for QDs, can be attributed to a very different dependence of the biexciton lifetimes on the sizes of the quantum confined and nonquantum confined dimensions, as demonstrated previously for CdSe NPLs.⁵¹ We propose that Auger recombination rates in 1D NRs and 2D NPLs depend on the product of binary collision frequency of excitons and Auger probability per collision. The observed linear dependence of biexciton Auger lifetimes in NPLs (NRs) on lateral area (rod length) can be attributed to the area (length)-dependent 2D (1D) exciton collision frequency. For NPLs and NRs with similar lengths and band-gaps, the biexciton Auger lifetime in NPLs is much longer than that in NRs, which is attributed to a reduced Auger probability per collision (P_{Aug}) in 2D materials. Compared to CdSe and PbSe NCs of the same dimensionalities and similar sizes, Auger recombination rates in 0D-2D CsPbBr₃ NCs are over 10-fold faster, which can be attributed to a larger Auger probability per collision (A_{Aug} for 0D and P_{Aug} for 1D and 2D) in CsPbBr₃ NCs. Our findings suggest that suppressing Auger recombination in CsPbBr3 NCs may be a fruitful approach to further improve their performance in optoelectronic devices, such as LED and lasers. Furthermore, the fast Auger recombination of CsPbBr₃ NCs may be exploited for other applications, such as Auger-assisted photon up-conversion.

Methods. Sample Synthesis. The colloidal CsPbBr₃ NPLs and NRs with different sizes were synthesized following the literature with slight modifications. ^{20,24,28,29} Detailed synthesis procedures are shown in the SI section S1.

Experimental Setup. Femtoseconds TA measurements were carried out by a regeneratively amplified Ti:sapphire laser system (Coherent Legend, 800 nm, 150 fs, 2.4 mJ/pulse, and 1 kHz repetition rate). The TA signals were collected and analyzed by the Helios system (Ultrafast Systems LLC). PL measurements were conducted with FluoroMax-3 spectro-fluorometer of HORIBA Scientific. Details of the experimental setup and optical characterizations of NPLs and NRs are shown in SI section S2.

■ ASSOCIATED CONTENT

S Supporting Information

The Supporting Information is available free of charge on the ACS Publications website at DOI: 10.1021/acs.nanolett.9b02145.

Synthesis procedures, additional sample characterizations, additional TA spectra and kinetics, fitting, and estimation details (PDF)

AUTHOR INFORMATION

Corresponding Author

*E-mail: tlian@emory.edu.

ORCID ®

Qiuyang Li: 0000-0002-8192-3960 Wenxiu Que: 0000-0002-0136-9710 Tianquan Lian: 0000-0002-8351-3690

Author Contributions

These authors contributed equally to this work.

Notes

The authors declare no competing financial interest.

ACKNOWLEDGMENTS

This work is funded by the National Science Foundation (CHE-1709182 and CHE-1726536 to T.L.), the National Natural Science Foundation of China (grant no. 61774122 to W.X.Q.), and the Science and Technology Developing Project of Shaanxi Province (grant no. 2015KW-001 to W.X.Q.). Y.Y. also acknowledges the financial support from the China Scholarship Council.

REFERENCES

- (1) Stranks, S. D.; Snaith, H. Nat. Nanotechnol. 2015, 10, 391-402.
- (2) Sutherland, B. R.; Sargent, E. H. Nat. Photonics 2016, 10, 295-302.
- (3) Zhao, Y.; Zhu, K. Chem. Soc. Rev. 2016, 45, 655-689.
- (4) Manser, J. S.; Christians, J. A.; Kamat, P. V. Chem. Rev. 2016, 116, 12956-13008.
- (5) Yang, W. S.; Noh, J. H.; Jeon, N. J.; Kim, Y. C.; Ryu, S.; Seo, J.; Seok, S. I. *Science* **2015**, *348*, 1234–1237.
- (6) Anaraki, E. H.; Kermanpur, A.; Steier, L.; Domanski, K.; Matsui, T.; Tress, W.; Saliba, M.; Abate, A.; Gratzel, M.; Hagfeldt, A.; Correa-Baena, J. P. *Energy Environ. Sci.* **2016**, *9*, 3128–3134.
- (7) Bi, D. Q.; Tress, W.; Dar, M. I.; Gao, P.; Luo, J. S.; Renevier, C.; Schenk, K.; Abate, A.; Giordano, F.; Baena, J. P. C.; Decoppet, J. D.; Zakeeruddin, S. M.; Nazeeruddin, M. K.; Gratzel, M.; Hagfeldt, A. Sci. Adv. 2016, 2, No. e1501170.
- (8) Momblona, C.; Gil-Escrig, L.; Bandiello, E.; Hutter, E. M.; Sessolo, M.; Lederer, K.; Blochwitz-Nimoth, J.; Bolink, H. J. *Energy Environ. Sci.* **2016**, *9*, 3456–3463.
- (9) Saliba, M.; Matsui, T.; Domanski, K.; Seo, J. Y.; Ummadisingu, A.; Zakeeruddin, S. M.; Correa-Baena, J. P.; Tress, W. R.; Abate, A.; Hagfeldt, A.; Gratzel, M. *Science* **2016**, *354*, 206–209.
- (10) Arora, N.; Dar, M. I.; Hinderhofer, A.; Pellet, N.; Schreiber, F.; Zakeeruddin, S. M.; Grätzel, M. Science 2017, 358, 768-771.
- (11) Shin, S. S.; Yeom, E. J.; Yang, W. S.; Hur, S.; Kim, M. G.; Im, J.; Seo, J.; Noh, J. H.; Seok, S. I. Science **2017**, 356, 167–171.
- (12) Stolterfoht, M.; Wolff, C. M.; Amir, Y.; Paulke, A.; Perdigon-Toro, L.; Caprioglio, P.; Neher, D. *Energy Environ. Sci.* **2017**, *10*, 1530–1539.
- (13) Tan, H. R.; Jain, A.; Voznyy, O.; Lan, X. Z.; de Arquer, F. P. G.; Fan, J. Z.; Quintero-Bermudez, R.; Yuan, M. J.; Zhang, B.; Zhao, Y. C.; Fan, F. J.; Li, P. C.; Quan, L. N.; Zhao, Y. B.; Lu, Z. H.; Yang, Z. Y.; Hoogland, S.; Sargent, E. H. *Science* **2017**, *355*, 722–726.
- (14) Yang, W. S.; Park, B. W.; Jung, E. H.; Jeon, N. J.; Kim, Y. C.; Lee, D. U.; Shin, S. S.; Seo, J.; Kim, E. K.; Noh, J. H.; Seok, S. I. *Science* **2017**, *356*, 1376–1379.
- (15) Diroll, B. T.; Zhou, H.; Schaller, R. D. Adv. Funct. Mater. 2018, 28, 1800945.

(16) Protesescu, L.; Yakunin, S.; Bodnarchuk, M. I.; Krieg, F.; Caputo, R.; Hendon, C. H.; Yang, R. X.; Walsh, A.; Kovalenko, M. V. *Nano Lett.* **2015**, *15*, 3692–3696.

- (17) Makarov, N. S.; Guo, S.; Isaienko, O.; Liu, W.; Robel, I.; Klimov, V. I. *Nano Lett.* **2016**, *16*, 2349–2362.
- (18) Akkerman, Q. A.; Abdelhady, A. L.; Manna, L. J. J. Phys. Chem. Lett. 2018, 9, 2326–2337.
- (19) Wu, K.; Liang, G.; Shang, Q.; Ren, Y.; Kong, D.; Lian, T. J. Am. Chem. Soc. 2015, 137, 12792–12795.
- (20) Amgar, D.; Stern, A.; Rotem, D.; Porath, D.; Etgar, L. Nano Lett. 2017, 17, 1007-1013.
- (21) Polavarapu, L.; Tong, Y.; Fu, M.; Bladt, E.; Huang, H.; Richter, A. F.; Wang, K.; Müller-Buschbaum, P.; Bals, S.; Tamarat, P.; Lounis, B.; Feldmann, J. *Angew. Chem., Int. Ed.* **2018**, *57*, 16094–16098.
- (22) Sun, S.; Yuan, D.; Xu, Y.; Wang, A.; Deng, Z. ACS Nano 2016, 10, 3648-3657.
- (23) Shamsi, J.; Dang, Z.; Bianchini, P.; Canale, C.; Di Stasio, F.; Brescia, R.; Prato, M.; Manna, L. J. Am. Chem. Soc. **2016**, 138, 7240–7243.
- (24) Akkerman, Q. A.; Motti, S. G.; Srimath Kandada, A. R.; Mosconi, E.; D'Innocenzo, V.; Bertoni, G.; Marras, S.; Kamino, B. A.; Miranda, L.; De Angelis, F.; Petrozza, A.; Prato, M.; Manna, L. *J. Am. Chem. Soc.* **2016**, *138*, 1010–1016.
- (25) Weidman, M. C.; Seitz, M.; Stranks, S. D.; Tisdale, W. A. ACS Nano 2016, 10, 7830-7839.
- (26) Weidman, M. C.; Goodman, A. J.; Tisdale, W. A. Chem. Mater. **2017**, 29, 5019–5030.
- (27) Hintermayr, V. A.; Polavarapu, L.; Urban, A. S.; Feldmann, J. ACS Nano 2018, 12, 10151–10158.
- (28) Shamsi, J.; Dang, Z.; Bianchini, P.; Canale, C.; Di Stasio, F.; Brescia, R.; Prato, M.; Manna, L. J. Am. Chem. Soc. **2016**, 138, 7240–7243.
- (29) Yang, Z.; Wang, M.; Qiu, H.; Yao, X.; Lao, X.; Xu, S.; Lin, Z.; Sun, L.; Shao, J. Adv. Funct. Mater. **2018**, 28, 1705908.
- (30) Li, Q.; Lian, T. J. Phys. Chem. Lett. 2019, 10, 566-573.
- (31) Li, J.; Luo, L.; Huang, H.; Ma, C.; Ye, Z.; Zeng, J.; He, H. J. Phys. Chem. Lett. **2017**, 8, 1161–1168.
- (32) Yang, D.; Zou, Y.; Li, P.; Liu, Q.; Wu, L.; Hu, H.; Xu, Y.; Sun, B.; Zhang, Q.; Lee, S.-T. *Nano Energy* **2018**, *47*, 235–242.
- (33) Cai, W.; Chen, Z.; Li, Z.; Yan, L.; Zhang, D.; Liu, L.; Xu, Q.-H.; Ma, Y.; Huang, F.; Yip, H.-L.; Cao, Y. ACS Appl. Mater. Interfaces **2018**, 10, 42564–42572.
- (34) Chiba, T.; Hayashi, Y.; Ebe, H.; Hoshi, K.; Sato, J.; Sato, S.; Pu, Y.-J.; Ohisa, S.; Kido, J. *Nat. Photonics* **2018**, *12*, 681–687.
- (35) Yan, F.; Xing, J.; Xing, G.; Quan, L.; Tan, S. T.; Zhao, J.; Su, R.; Zhang, L.; Chen, S.; Zhao, Y.; Huan, A.; Sargent, E. H.; Xiong, Q.; Demir, H. V. *Nano Lett.* **2018**, *18*, 3157–3164.
- (36) Zhang, X. Y.; Lin, H.; Huang, H.; Reckmeier, C.; Zhang, Y.; Choy, W. C. H.; Rogach, A. L. *Nano Lett.* **2016**, *16*, 1415–1420.
- (37) Song, J. Z.; Li, J. H.; Li, X. M.; Xu, L. M.; Dong, Y. H.; Zeng, H. B. Adv. Mater. 2015, 27, 7162–7167.
- (38) Xiao, Z.; Kerner, R. A.; Zhao, L.; Tran, N. L.; Lee, K. M.; Koh, T.-W.; Scholes, G. D.; Rand, B. P. *Nat. Photonics* **2017**, *11*, 108–115.
- (39) Lee, J.-W.; Choi, Y. J.; Yang, J.-M.; Ham, S.; Jeon, S. K.; Lee, J. Y.; Song, Y.-H.; Ji, E. K.; Yoon, D.-H.; Seo, S.; Shin, H.; Han, G. S.; Jung, H. S.; Kim, D.; Park, N.-G. ACS Nano 2017, 11, 3311–3319.
- (40) Geiregat, P.; Maes, J.; Chen, K.; Drijvers, E.; De Roo, J.; Hodgkiss, J. M.; Hens, Z. ACS Nano 2018, 12, 10178–10188.
- (41) Wang, Y.; Li, X.; Song, J.; Xiao, L.; Zeng, H.; Sun, H. Adv. Mater. 2015, 27, 7101–7108.
- (42) Xu, Y.; Chen, Q.; Zhang, C.; Wang, R.; Wu, H.; Zhang, X.; Xing, G.; Yu, W. W.; Wang, X.; Zhang, Y.; Xiao, M. J. Am. Chem. Soc. **2016**, 138, 3761–3768.
- (43) Yakunin, S.; Protesescu, L.; Krieg, F.; Bodnarchuk, M. I.; Nedelcu, G.; Humer, M.; De Luca, G.; Fiebig, M.; Heiss, W.; Kovalenko, M. V. *Nat. Commun.* **2015**, *6*, 8056.
- (44) Su, R.; Diederichs, C.; Wang, J.; Liew, T. C. H.; Zhao, J.; Liu, S.; Xu, W.; Chen, Z.; Xiong, Q. *Nano Lett.* **2017**, *17*, 3982–3988.

(45) Klimov, V. I.; Mikhailovsky, A. A.; McBranch, D. W.; Leatherdale, C. A.; Bawendi, M. G. Science 2000, 287, 1011–1013.

- (46) Robel, I.; Gresback, R.; Kortshagen, U.; Schaller, R. D.; Klimov, V. I. *Phys. Rev. Lett.* **2009**, *102*, 177404.
- (47) Lim, J.; Park, Y.-S.; Klimov, V. I. Nat. Mater. 2018, 17, 42-49.
- (48) Grim, J. Q.; Christodoulou, S.; Di Stasio, F.; Krahne, R.; Cingolani, R.; Manna, L.; Moreels, I. *Nat. Nanotechnol.* **2014**, *9*, 891–895
- (49) She, C. X.; Fedin, I.; Dolzhnikov, D. S.; Demortiere, A.; Schaller, R. D.; Pelton, M.; Talapin, D. V. *Nano Lett.* **2014**, *14*, 2772–2777
- (50) Klimov, V. I.; Ivanov, S. A.; Nanda, J.; Achermann, M.; Bezel, I.; McGuire, J. A.; Piryatinski, A. *Nature* **2007**, *447*, 441–446.
- (51) Li, Q.; Lian, T. Nano Lett. 2017, 17, 3152-3158.
- (52) Dang, Z.; Shamsi, J.; Palazon, F.; Imran, M.; Akkerman, Q. A.; Park, S.; Bertoni, G.; Prato, M.; Brescia, R.; Manna, L. ACS Nano **2017**, 11, 2124–2132.
- (53) Zhai, W.; Lin, J.; Li, Q.; Zheng, K.; Huang, Y.; Yao, Y.; He, X.; Li, L.; Yu, C.; Liu, C.; Fang, Y.; Liu, Z.; Tang, C. Chem. Mater. **2018**, 30, 3714–3721.
- (54) Li, Y.; Ding, T.; Luo, X.; Chen, Z.; Liu, X.; Lu, X.; Wu, K. Nano Res. 2019, 12, 619–623.
- (55) Padilha, L. A.; Stewart, J. T.; Sandberg, R. L.; Bae, W. K.; Koh, W.-K.; Pietryga, J. M.; Klimov, V. I. *Nano Lett.* **2013**, *13*, 1092–1099.
- (56) McGuire, J. A.; Sykora, M.; Robel, I.; Padilha, L. A.; Joo, J.; Pietryga, J. M.; Klimov, V. I. ACS Nano 2010, 4, 6087–6097.
- (57) Midgett, A. G.; Hillhouse, H. W.; Hughes, B. K.; Nozik, A. J.; Beard, M. C. J. Phys. Chem. C 2010, 114, 17486–17500.
- (58) Padilha, L. A.; Robel, I.; Lee, D. C.; Nagpal, P.; Pietryga, J. M.; Klimov, V. I. *ACS Nano* **2011**, *5*, 5045–5055.
- (59) Kunneman, L. T.; Tessier, M. D.; Heuclin, H.; Dubertret, B.; Aulin, Y. V.; Grozema, F. C.; Schins, J. M.; Siebbeles, L. D. A. *J. Phys. Chem. Lett.* **2013**, *4*, 3574–3578.
- (60) Robel, I.; Gresback, R.; Kortshagen, U.; Schaller, R. D.; Klimov, V. I. *Phys. Rev. Lett.* **2009**, *102*, 177404.
- (61) Padilha, L. A.; Stewart, J. T.; Sandberg, R. L.; Bae, W. K.; Koh, W. K.; Pietryga, J. M.; Klimov, V. I. *Acc. Chem. Res.* **2013**, *46*, 1261–1269.
- (62) Schaller, R. D.; Klimov, V. I. Phys. Rev. Lett. 2004, 92, 186601.
- (63) Schaller, R. D.; Pietryga, J. M.; Klimov, V. I. Nano Lett. 2007, 7, 3469–3476.
- (64) Dyakonov, M. I.; Kachorovskii, V. Y. Phys. Rev. B: Condens. Matter Mater. Phys. 1994, 49, 17130–17138.
- (65) Wang, F.; Wu, Y.; Hybertsen, M. S.; Heinz, T. F. Phys. Rev. B: Condens. Matter Mater. Phys. 2006, 73, 245424.
- (66) Feldmann, J.; Peter, G.; Göbel, E. O.; Dawson, P.; Moore, K.; Foxon, C.; Elliott, R. J. *Phys. Rev. Lett.* **1987**, *59*, 2337–2340.
- (67) Ma, X.; Diroll, B. T.; Cho, W.; Fedin, I.; Schaller, R. D.; Talapin, D. V.; Gray, S. K.; Wiederrecht, G. P.; Gosztola, D. J. ACS Nano 2017, 11, 9119–9127.
- (68) Li, Q.; Liu, Q.; Schaller, R. D.; Lian, T. J. Phys. Chem. Lett. 2019, 10, 1624-1632.
- (69) Brus, L. E. J. Chem. Phys. 1983, 79, 5566-5571.
- (70) Philbin, J. P.; Rabani, E. Nano Lett. 2018, 18, 7889-7895.
- (71) Mahler, B.; Nadal, B.; Bouet, C.; Patriarche, G.; Dubertret, B. J. Am. Chem. Soc. **2012**, 134, 18591–18598.
- (72) Taguchi, S.; Saruyama, M.; Teranishi, T.; Kanemitsu, Y. Phys. Rev. B: Condens. Matter Mater. Phys. 2011, 83, 155324.
- (73) Htoon, H.; Hollingsworth, J. A.; Dickerson, R.; Klimov, V. I. *Phys. Rev. Lett.* **2003**, *91*, 227401.
- (74) Ithurria, S.; Tessier, M. D.; Mahler, B.; Lobo, R. P. S. M.; Dubertret, B.; Efros, A. *Nat. Mater.* **2011**, *10*, 936–941.
- (75) Vaxenburg, R.; Rodina, A.; Shabaev, A.; Lifshitz, E.; Efros, A. L. *Nano Lett.* **2015**, *15*, 2092–2098.
- (76) Xiao, P.; Huang, J.; Yan, D.; Luo, D.; Yuan, J.; Liu, B.; Liang, D. *Materials* **2018**, *11*, 1376.
- (77) Qin, C.; Matsushima, T.; Sandanayaka, A. S. D.; Tsuchiya, Y.; Adachi, C. J. J. Phys. Chem. Lett. 2017, 8, 5415-5421.

(78) Fan, F.; Kanjanaboos, P.; Saravanapavanantham, M.; Beauregard, E.; Ingram, G.; Yassitepe, E.; Adachi, M. M.; Voznyy, O.; Johnston, A. K.; Walters, G.; Kim, G.-H.; Lu, Z.-H.; Sargent, E. H. *Nano Lett.* **2015**, *15*, 4611–4615.

- (79) Chen, Z.; Nadal, B.; Mahler, B.; Aubin, H.; Dubertret, B. Adv. Funct. Mater. **2014**, 24, 295–302.
- (80) Liu, B.; Delikanli, S.; Gao, Y.; Dede, D.; Gungor, K.; Demir, H. V. Nano Energy **2018**, 47, 115–122.
- (81) Vitukhnovsky, A. G.; Lebedev, V. S.; Selyukov, A. S.; Vashchenko, A. A.; Vasiliev, R. B.; Sokolikova, M. S. *Chem. Phys. Lett.* **2015**, *619*, 185–188.
- (82) Eperon, G. E.; Jedlicka, E.; Ginger, D. S. J. Phys. Chem. Lett. **2018**, 9, 104–109.
- (83) Makarov, N. S.; Lin, Q.; Pietryga, J. M.; Robel, I.; Klimov, V. I. ACS Nano **2016**, 10, 10829–10841.
- (84) Teitelboim, A.; Oron, D. ACS Nano 2016, 10, 446-452.
- (8S) Rainò, G.; Nedelcu, G.; Protesescu, L.; Bodnarchuk, M. I.; Kovalenko, M. V.; Mahrt, R. F.; Stöferle, T. ACS Nano 2016, 10, 2485–2490.
- (86) Fu, M.; Tamarat, P.; Trebbia, J.-B.; Bodnarchuk, M. I.; Kovalenko, M. V.; Even, J.; Lounis, B. *Nat. Commun.* **2018**, *9*, 3318. (87) Trinh, C. T.; Minh, D. N.; Ahn, K. J.; Kang, Y.; Lee, K.-G. *ACS Photonics* **2018**, *5*, 4937–4943.